International Journal of Heat and Fluid Flow 30 (2009) 44–53

Contents lists available at ScienceDirect

International Journal of Heat and Fluid Flow

journal homepage: www.elsevier.com/locate/ijhff

Numerical modeling of cryogenic chilldown process in terrestrial gravity and microgravity

Kun Yuan, Yan Ji, J.N. Chung *

Department of Mechanical and Aerospace Engineering, University of Florida, P.O. Box 116300, Gainesville, FL 32611-6300, USA

ARTICLE INFO

Article history:
Received 13 November 2007
Received in revised form 5 October 2008
Accepted 11 October 2008
Available online 6 December 2008

Keywords:
Chilldown
Quenching
Dispersed flow
Film boiling
Heat transfer
Cryogenics

ABSTRACT

In this paper, a numerical model is developed to predict the cryogenic chilldown process of a vertical tube for both terrestrial and microgravity conditions. The flow field is covered by four distinct regions, which are single-phase vapor region, dispersed flow region, inverted annular flow region, and single-phase liquid region. Heat transfer mechanisms are dictated by the flow patters. A two-fluid model is employed to analyze the dispersed flow region and the inverted annular film boiling region. Gravity effect on the chilldown process is also investigated. Model results indicate that film boiling heat transfer decreases with decreasing gravity level for the bottom flooding condition. The model results show a good agreement with the experimental data.

1. Introduction

One important application of cryogenic fluids is in space exploration. Efficient and safe use of cryogenic fluids in thermal management, power and propulsion, and life-support systems of a spacecraft during space missions involves transport, handling, and storage of these fluids under both terrestrial and microgravity conditions. Uncertainties about the flow pattern and heat transfer characteristics pose severe design concerns. For any process using cryogenic fluids, chilldown is inevitably the initial stage; therefore, efficiency of the chilldown process is a significant concern since the cryogen used to cool down the piping system cannot be utilized for propulsion, power generation or other applications. In a hydrogen economy, chilldown must be accomplished with a minimum consumption of cryogen in order for the overall energy efficiency to stay within tolerable limits.

Previous experimental studies of cryogenic chilldown process were mainly carried out under the 1-g condition. Among such published studies one should mention the works of Burke et al. (1960), Bronson et al. (1962), Kawaji et al. (1985). However, in the studies of comparing vertical tube chilldown under both normal and reduced gravity conditions, we were able to find just one report by Antar and Collins (1997) due to the extreme difficulties in conducting such experiments. Westbye et al. (1995) investigated the quenching of a horizontal tube under microgravity. In their experiment, the flow pattern observed before microgravity was a stratified flow. They found that the film boiling heat transfer coefficients in microgravity were only 20–50% of those obtained in 1 g and they also reported lower rewetting temperature under microgravity.

The only microgravity chilldown experimental results were reported in Westbye et al. (1995), Kawaji et al. (1991) for R-113 coolant and in Antar and Collins (1997) for liquid nitrogen coolant. However, only Kawaji et al. (1991), Antar and Collins (1997) reported two-phase flow patterns. Both papers mentioned that evaporating liquid filaments flowed in the central region of the tube and were surround by vapor that filled in the space between the tube wall and the liquid filaments. Both also noted that liquid cannot touch the wall and inverted annular flow predominated right after the liquid entered the tube. We believe that it is a strong evidence of an inverted annular flow. In the experiment by Antar and Collins (1997), the liquid nitrogen was in the saturated state when injected into the tube. Therefore, saturated inverted annular flow was reported to exist in Antar and Collins (1997).

In the modeling aspect, a homogeneous model prevailed in early works (e.g. Burke et al., 1960; Bronson et al., 1962; Chi, 1965), in which the two-phases were assumed at thermal-equilibrium. However, later understanding of boiling heat transfer systems showed that post critical heat flux (CHF) heat transfer

Abbreviations: CHF, critical heat flux; DFFB, dispersed flow film boiling; QF, Quenching front; IAF, inverted annular flow; IAFB, inverted annular film boiling.

* Corresponding author. Tel.: +1 352 392 9607; fax: +1 352 392 1071.
E-mail address: jnchung@ufl.edu (J.N. Chung).

0142-727X/$ - see front matter © 2008 Elsevier Inc. All rights reserved.
doi:10.1016/j.ijheatfluidflow.2008.10.004

Nomenclature

A	area [m^2]
C_D	Drag coefficient
C_p	specific heat capacity [J kg^{-1} K^{-1}]
d	diameter of liquid droplets [m]
D	diameter of the flow channel [m]
E	liquid droplet entrainment fraction
f	friction factor
F_D	drag force [N]
g	gravitational acceleration constant 9.8 [ms^{-2}]
h	heat transfer coefficient [W m^{-2} K^{-1}]; enthalpy [J kg^{-1}]
h_{lv}	latent heat of evaporation [J kg^{-1}]
h'_{lv}	modified latent heat [J kg^{-1}]
k	thermal conductivity [W m^{-1} K^{-1}]
m''_l	mass transfer rate per unit area [kg m^{-2} s^{-1}]
m'''_l	mass transfer rate per unit volume [kg m^{-3} s^{-1}]
Nu	Nusselt number
P	pressure [Pa] ; perimeter [m]
Pr	Prandtl number
q''	heat flux [W m^{-2}]
R	radius of the flow channel [m]
R_g	gas constant
Re	Reynolds number
t	time [s]
T	temperature [K]
u	velocity [m s^{-1}]
X_{tt}	Martinelli parameter
z	position

Greek letters

α	void fraction; Thermal diffusivity [m^2 s^{-1}]
δ	vapor film thickness [m]
ε	emissivity
μ	viscosity [kg m^{-1} s^{-1}]
ρ	density [kg m^{-3}]
σ	surface tension [N m^{-1}]
σ_B	Stefan Boltzmann constant 5.67×10^{-8} [W m^{-2} K^{-4}]
τ	shear stress [N m^{-2}]

Subscripts

2φ	two-phase
d	droplet
ev	evaporation
evap	evaporation
i	interfacial
l	liquid phase
lh	liquid heating
ls	liquid saturated
pool	pool boiling
r	radiation
s	saturation
v	vapor phase
vd	vapor to droplet
vl	vapor to liquid
vs	vapor saturated
w	wall
wd	wall to droplet
wv	wall to vapor

Superscripts

$''$	quantity per unit area
$'''$	quantity per unit volume

should be more concerned with non-equilibrium between the two phases (Chen et al., 1979). For the inverted annular film boiling (IAFB) and dispersed flow film boiling (DFFB), the vapor phase is generally superheated (e.g., Guo et al., 2002; Tian et al., 2006; Chan and Banerjee, 1981a). The vapor superheat can be up to several hundred Kelvin under some operating conditions. In that situation, predictions by the homogeneous model will inevitably lead to a large discrepancy from the experimental results. Therefore, a multifield model has been developed to account for the non-equilibrium effects. A two-fluid version was successfully used by Chan and Banerjee (1981a, 1981b) for the prediction of refilling and rewetting of a horizontal tube. This model was further extended by Liao et al. (2005) for a cryogenic chilldown process in a horizontal tube. For a vertical tube, Kawaji et al. (1987, 1988) and Hedayatpour et al. (1993) adopted this model to predict the thermohydraulic criteria for the bottom flooding problem.

However, there is no related modeling work for a chilldown process under different gravity levels. Therefore, in the present study, a two-fluid model based on experimental observations was developed to investigate a vertical tube cryogenic chilldown process under different gravity conditions. The gravity effects on the temperature development and cooling rate are also investigated.

2. Model description

2.1. Flow patterns and heat transfer regimes during the chilldown process

Since different heat transfer mechanisms are associated with different flow patterns, therefore the first step in modeling the chilldown process should be a correct description of the flow pattern sequence and the corresponding transition criteria.

Antar and Collins (1997), Yuan et al. (2005, 2007) conducted chilldown experiments under different gravity conditions and obtained similar observations. Initially, the tube wall temperature is usually much higher than the liquid boiling saturation temperature. When the cryogenic flow first enters the hot tube, as the tube wall temperature is much higher than the Leindenfrost point, the liquid phase evaporates very quickly and forms a vapor film that prevents the liquid phase from touching the tube wall, and the two-phase flow is usually in an inverted annular flow (IAF) state, the corresponding heat transfer regime is inverted annular film boiling (IAFB). The local void fraction and interfacial shear increase as the two-phase flow travels further downstream, this will lead the two-phase flow pattern to change to a dispersed flow, in which the liquid phase is dispersed in a continuous vapor phase. Further heat transfer to the dispersed flow will evaporate all the liquid droplets and result in a pure vapor flow. On the other hand, the wall temperature keeps decreasing during the chilldown process, at a certain point, which is often called "wall rewetting", the liquid phase is able to wet the tube wall. The liquid-wall contact front, which is often referred to as the quenching front (QF) or sputtering region, is characterized by violent boiling associated with a significant wall temperature decrease. The quenching front propagates downstream with the flow. The heat transfer mechanism at the QF is transition boiling, which is more effective than the film boiling heat transfer. After the QF, nucleate boiling heat transfer dominates. With a further wall temperature decrease, the nucleate boiling stage gradually changes to pure single-phase convection until the wall temperature reaches the steady state, which denotes the end of the chilldown process.

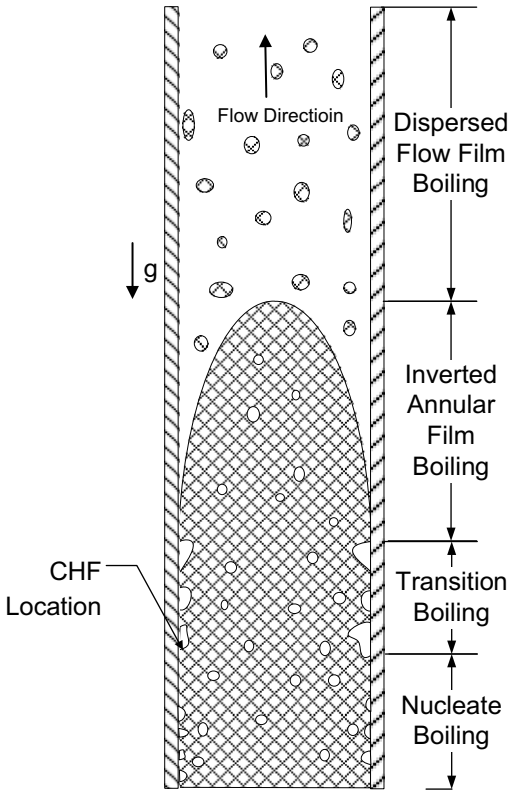

Fig. 1. Flow pattern sequence of cryogenic chilldown model.

On the basis of these experimental observations, the sequence of the cryogenic chilldown flow pattern begins with the pure vapor flow far downstream and followed by dispersed flow, inverted annular flow, and pure liquid flow as shown in Fig. 1. This sequence has been verified in other vertical cryogenic chilldown experiments (Kawaji et al, 1985; Laverty et al., 1967), and was adopted in other two-fluid models (Kawaji et al., 1987; Kawaji et al., 1988).

2.2. Mathematical formulation

For the flow pattern sequence described in the previous section, the most difficult part of the current model is how to correctly predict the thermohydraulic characteristics of the two-phase flow regions, namely the IAFB region and dispersed flow region. Two-fluid formulations are used for these two regions, in which each phase is described by one set of conservation equations and some interaction terms between the two phases appearing in the field equations as source terms. Different constitutive relations in previous literatures (e.g., Guo et al., 2002; Tian et al., 2006; Kawaji, et al., 1987; Hedayatpour et al., 1993; Analytis et al., 1987; Hammouda et al., 1997) are compared and selected to close the model. Formulations for other regions in the tube are relatively simple. Regions in the upstream of QF and downstream of dispersed flow are modeled as pure liquid flow and pure vapor flow, respectively. For the tube wall temperature prediction, a one-dimensional energy equation is used.

2.2.1. Inverted annular film boiling (IAFB) regime

IAFB is characterized by a high surface temperature and consists of a continuous liquid core at the center of the channel and a vapor blanket covering the heated surface, as shown in Fig. 2a. Conservation equations for the IAFB model are derived based on the following assumptions: (1) liquid flows in the center of the flow channel and is separated from the heated wall by a vapor layer. The vapor layer thickness $\delta(z)$ is uniform along the tube periphery; (2) the vapor layer contains no entrained liquid, and the liquid core contains no vapor bubbles; (3) the pressure is uniform in the radial direction, and the two phases are in thermodynamic non-equilibrium; the vapor phase is treated as an ideal gas; (4) the interface is smooth and in saturated condition.

For a vertical tube, the transient one-dimensional two-fluid equations for the IAFB region can be derived based on the one-dimensional two-fluid forms:

Continuity equations:

$$\frac{\partial}{\partial t}(\alpha\rho)_l + \frac{\partial}{\partial z}(\alpha\rho u)_l = -m_l'' \frac{P_i}{A} \tag{1}$$

$$\frac{\partial}{\partial t}(\alpha\rho)_v + \frac{\partial}{\partial z}(\alpha\rho u)_v = m_l'' \frac{P_i}{A} \tag{2}$$

Momentum equations:

$$\frac{\partial}{\partial t}(\alpha\rho u)_l + \frac{\partial}{\partial z}(\alpha\rho uu)_l + \alpha_l \frac{dP}{dz} = \pm\alpha_l\rho_l g + \frac{\tau_i P_i}{A} \tag{3}$$

$$\frac{\partial}{\partial t}(\alpha\rho u)_v + \frac{\partial}{\partial z}(\alpha\rho uu)_v + \alpha \frac{dP}{dz} = \pm\alpha\rho_v g - \frac{\tau_i P_i}{A} - m_l'' \frac{(u_v - u_l)P_i}{A} - \frac{\tau_{wv} P_w}{A} \tag{4}$$

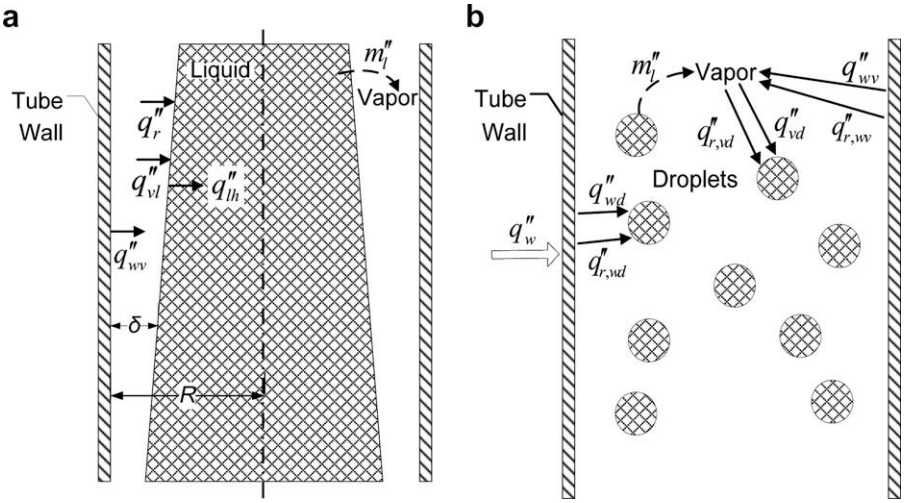

Fig. 2. Model of the two-phase regions in chilldown experiments: (a) inverted annular film boiling region (b) dispersed flow region.

Enthalpy energy equations:

$$\frac{\partial}{\partial t}(\alpha\rho h)_l + \frac{\partial}{\partial z}(\alpha\rho u h)_l = -m_l''\frac{(h_{ls}-h_l)P_i}{A} \quad (5)$$

$$\frac{\partial}{\partial t}(\alpha\rho h)_v + \frac{\partial}{\partial z}(\alpha\rho u h)_v = \frac{q_v''P_i}{A} + m_l''\frac{(h_{vs}-h_v)P_i}{A} \quad (6)$$

Here, m_l'' denotes the vaporization mass flux at the interface. τ_i and τ_{wv} are the interfacial shear stress and wall to vapor shear stress, respectively. q_v'' is the heat flux used to heat up the vapor. For the body force terms in the momentum equations, the plus sign is for downward flow, and the minus sign is for upward flow, and body force terms are considered as zero in 0-g calculations.

Based on the above assumptions, the vapor layer thickness can be expressed as a function of tube radius R and the void fraction α:

$$\delta = R\left(1-\sqrt{1-\alpha}\right) \quad (7)$$

and the cross-sectional area, interfacial and inside tube wall peripheral lengths as

$$A = \pi R^2 \quad (8)$$

$$P_i = 2\pi(R-\delta) \quad (9)$$

$$P_w = 2\pi R \quad (10)$$

Empirical relations of the shear stress and heat and mass flux terms should be provided to close Eqs. (1)–(6). As shown in Fig. 2a, the total heat flux received by the liquid column is

$$q_l'' = q_{vl}'' + q_r'' \quad (11)$$

where q_{vl}'' is the vapor–liquid convection heat flux and q_r'' is the radiation heat flux directly from the wall. While the energy balance for the vapor phase gives

$$P_i q_v'' = q_{wv}'' P_w - q_{vl}'' P_i \quad (12)$$

Here q_{wv}'' is the wall to vapor convection heat flux; the interfacial and wall perimeter appear in the above equation due to the difference in heat transfer areas. Since the total heat flux to the liquid phase is used to evaporate the liquid at interface, the vapor evaporation heat flux q_{ev}'' is

$$q_{ev}'' = q_l'' = q_{vl}'' + q_r'' \quad (13)$$

The vapor generation term m_l'', which denotes the vapor generation rate per unit area at the interface, can be expressed as

$$m_l'' = q_{ev}''/h_{lv} \quad (14)$$

where h_{lv} is the latent heat for phase change.

Empirical correlations are applied to evaluate the heat transfer and shear stress terms. In this work, if $\delta \ll R$, we follow the previous approaches (Kawaji et al., 1988; Analytis et al., 1987) by considering the vapor flow as flow between two parallel plates, the wall to vapor and vapor to liquid heat fluxes can be given as (Kays, 1993)

$$q_{wv}'' = \frac{k_v \mathrm{Nu}_w}{2\delta(1-\theta^{*2})}[(T_w - T_v) - \theta^*(T_v - T_s)] \quad (15)$$

$$q_{vl}'' = \frac{k_v \mathrm{Nu}_i}{2\delta(1-\theta^{*2})}[(T_v - T_s t) - \theta^*(T_w - T_v)] \quad (16)$$

where θ^* is the influence coefficient. Kays (1993) gave that for laminar flow $\mathrm{Nu} = 5.385$ and $\theta^* = 0.346$; for turbulent flow with Re = 10,000, Nu = 27.8 and $\theta^* = 0.220$ (for Pr = 0.7). The Nusselt number Nu and θ^* can be interpolate between the laminar values and turbulent values for $\delta \ll R$.

While, for $\delta \sim R$, the Colburn equation (Incropera and DeWitt, 2002) is used

$$q_{wv}'' = 0.023\frac{k_v}{2\delta}\mathrm{Re}_w^{0.8}\mathrm{Pr}_v^{0.33}(T_w - T_v) \quad (17)$$

$$q_{vl}'' = 0.023\frac{k_v}{2\delta}\mathrm{Re}_i^{0.8}\mathrm{Pr}_v^{0.33}(T_v - T_l) \quad (18)$$

and the Reynolds numbers are defined as

$$\mathrm{Re}_w = \rho_v u_v 2\delta/\mu_v \quad (19)$$

$$\mathrm{Re}_i = \rho_v |u_v - u_l| 2\delta/\mu_v \quad (20)$$

in which, μ_v is the vapor viscosity. Assuming that the vapor film is transparent to thermal radiation and the wall is gray, the radiation heat flux to the liquid core can be expressed as (Hammouda et al., 1997)

$$q_r'' = \frac{\sigma_B(T_w^4 - T_s^4)}{\frac{1}{\varepsilon_w} + \frac{1}{\varepsilon_l\sqrt{\alpha_l}} - 1} \quad (21)$$

where σ_B is the Stefan–Boltzmann constant; ε_w and ε_l are emissivities of the wall and the liquid, respectively. For a turbulent flow in the vapor film, different correlations have been suggested for wall shear stress and interfacial shear stress; here we adopt those used by Kawaji and Banerjee (1988), which have the same form for the two stresses:

$$\tau_{wv} = 0.5 f_w \rho_v u_v^2 \quad (22)$$

$$\tau_i = 0.5 f_i \rho_v (u_v - u_l)^2 \quad (23)$$

where f_w and f_i are friction factors, and given by

$$f_w = 0.085\mathrm{Re}_w^{-0.25} \quad (24)$$

$$f_i = 0.085\mathrm{Re}_i^{-0.25} \quad (25)$$

in which Re_w and Re_i are the same as those defined in Eq. (19) and (20), respectively.

2.2.2. Dispersed flow region

In chilldown experiments, with increasing void fraction and velocity difference between the two phases, dispersed flow is expected to appear downstream of the IAFB region. Assumptions to derive the conservation equations for dispersed flow are listed as follows: (1) the liquid phase is dispersed spherical droplets, while the vapor phase is continuous; (2) the two phases are in thermodynamic non-equilibrium, the liquid phase is at saturation temperature, and the vapor phase is treated as ideal gas; (3) the vapor and liquid pressures are uniform and equal to the tube exit pressure; (4) at any given cross-section of the flow channel, all droplets have the same diameter d. The droplet diameter is a function of axial position or void fraction α; (5) at any given cross-section of the flow channel, all droplets move with the same velocity u_d; (6) the interfacial velocity is the same as the droplet velocity. Here, the assumption (3) is adopted from previous work (Hedayatpour et al., 1993) and based on the fact that the pressure drop in the dispersed region is very small compared with the total pressure drop. Under this assumption, the pressure is not an unknown, and the vapor momentum equation does not need to be solved, therefore the problem is significantly simplified.

For a vertical tube, the transient one-dimensional two-fluid equations for the dispersed flow region are given as below:

Continuity equation:

$$\frac{\partial}{\partial t}(\alpha_l\rho_l) + \frac{\partial}{\partial z}(\alpha_l\rho_l u_d) = -m_l''' \quad (26)$$

$$\frac{\partial}{\partial t}(\alpha\rho_v) + \frac{\partial}{\partial z}(\alpha\rho_v u_v) = m_l''' \quad (27)$$

Momentum equation:

$$\frac{\partial}{\partial t}(\alpha_l\rho_l u_d) + \frac{\partial}{\partial z}(\alpha_l\rho_l u_d u_d) = \pm\alpha_l\rho_l g + \tau_d''' \quad (28)$$

Vapor enthalpy equation:

$$\frac{\partial}{\partial t}(\alpha\rho_v h_v) + \frac{\partial}{\partial z}(\alpha\rho_v u_v h_v) = q_v''' + m_l'''(h_{vs} - h_v) \quad (29)$$

Vapor state equation:

$$\rho_v = \frac{P}{R_g} T_v \tag{30}$$

In the above equations, subscript d is for liquid phase, v is for vapor phase and s denotes saturation; m_l''' is the interfacial mass transfer rate per unit volume; q_v''' is the heat used to heat up the vapor per unit volume; τ_d''' is the shear stress on liquid droplets; for the body force in the momentum equations, again plus sign is for down-flow, minus sign is for up-flow, and body force terms are considered as zero in 0-g calculations.

Heat and mass transfer in the dispersed flow region is rather complex. Since the two phases are generally in thermal non-equilibrium, possible heat and mass transfer processes are considered as follows (Guo, et al., 2002; Andreani et al., 1994), which are illustrated in Fig. 2b: (1) convective heat transfer from the wall to the vapor q_{wv}''; (2) interfacial heat transfer between the vapor and droplets q_{vd}''; (3) direct contact wall-to-droplet heat transfer q_{wd}''; (4) radiative heat transfer from the wall to the droplets $q_{r,wd}''$; (5) radiative heat transfer from the wall to the vapor $q_{r,wv}''$; (6) radiative heat transfer from the vapor to the droplets $q_{r,vd}''$; (7) evaporation mass flux of the droplets m_l''.

Similar to the IAFB model, constitutive relations for heat and mass transfer and shear stress terms need to be provided to close the model. In the present work, we have investigated the previous researches and selected the most acceptable correlations, which will be given below. The convective heat transfer from the wall to the vapor q_{wv}'' contributes most to the total heat removal from the wall, and is modeled as below (Hedayatpour et al., 1993; Ganić et al., 1977)

$$Q_{wv}'' = 0.023 \frac{k_v}{D} \mathrm{Re}_v^{0.8} \mathrm{Pr}_v^{0.33} (T_w - T_v) \tag{31}$$

where D is the tube ID and Re_v is the vapor Reynolds number. The interfacial heat transfer between vapor and droplets is calculated by the Lee–Ryley model (Kawaji, et al., 1988; Lee et al., 1968):

$$q_{vd}'' = \frac{k_v}{d} (2 + 0.74 \mathrm{Re}_d^{0.5} \mathrm{Pr}_v^{0.33}) (T_v - T_s) \tag{32}$$

here d is the droplet diameter, and Re_d is the droplet Reynolds number defined as

$$\mathrm{Re}_d = \frac{\rho_v (u_v - u_d) d}{\mu_v} \tag{33}$$

The direct contact wall-to-droplet heat transfer is usually much smaller than the convective heat transfer from the wall to the vapor, and is modeled by (Guo et al., 2002)

$$q_{wd}'' = \left[\frac{18 k_v^3 t_R^3 \rho_v h_{lv}' \dot{m}_d^5}{d^5 \rho_l^4 \mu_v (1-\alpha)(T_w - T_s)} \right]^{1/4} (T_w - T_s) \tag{34}$$

where $h_{lv}' = h_{lv} + C_p(T_v - T_s)$, is the modified latent heat; t_R is the droplet resident time, which characterizes the average time that the droplet is in contact with the wall, and is given by Bolle and Moureau (Bolle et al., 1986) as

$$t_R = \pi \sqrt{\rho_l d^3 d^3 16 \sigma} \tag{35}$$

In Eq. (34), $\dot{m}_d$ is the deposition rate, which represents the droplet mass impinging rate on the wall per unit area, and is given by Kataoka and Ishii (1983) as

$$\dot{m}_d = K(1-\alpha)\rho_l \tag{36}$$

where K is the deposition mass transfer coefficient and given as

$$K = \frac{\mu_l}{D} 0.22 \mathrm{Re}_l 0.74 \left(\frac{\mu_v}{\mu_l} \right) \tag{37}$$

here E denotes the fraction of liquid droplet entrainment in the vapor core and equals to unity for the dispersed flow. Also σ and α are surface tension and void fraction, respectively.

In general, the radiation heat transfer among the wall, the vapor and the droplet is usually small. If this effect is considered, the method proposed by Sun et al. (1976) is applied here. The wall, the vapor, and the droplets are characterized by an electrical network as shown in Fig. 3. The radiation heat fluxes can then be expressed as

$$q_{r,wv}'' = (R_w + R_v + R_w R_v / R_d)^{-1} \sigma_B (T_w^4 - T_v^4) \tag{38}$$

$$q_{r,wd}'' = (R_w + R_d + R_w R_d / R_d)^{-1} \sigma_B (T_w^4 - T_s^4) \tag{39}$$

$$q_{r,vd}'' = (R_v + R_d + R_v R_d / R_w)^{-1} \sigma_B (T_v^4 - T_s^4) \tag{40}$$

where

$$R_v = (1 - \varepsilon_v) / [\varepsilon_v (1 - \varepsilon_v \varepsilon_d)] \tag{41}$$

$$R_d = (1 - \varepsilon_d) / [\varepsilon_d (1 - \varepsilon_v \varepsilon_d)] \tag{42}$$

$$R_w = 1 / (1 - \varepsilon_v \varepsilon_d) + (1 - \varepsilon_w) / \varepsilon_w \tag{43}$$

In the above equations, ε_w, ε_v and ε_d are emissivities of the wall, the vapor and the droplets, respectively.

Note that all the heat absorbed by the liquid phase is assumed to be used to evaporate the liquid droplets. On the basis of energy balance, the heat used to evaporate the droplets per unit volume is given by

$$q_{\mathrm{evap}}''' = A_i''' q_{vd}'' + \frac{4}{D} (q_{r,vd}'' + q_{wd}'' + q_{r,wd}'') \tag{44}$$

Therefore, the interfacial mass transfer rate per unit volume in the model equations is

$$m_l''' = q_{\mathrm{evap}}''' / h_{lv} \tag{45}$$

Here A_i''' is the interfacial area per unit volume of the flow channel, which is given as

$$A_i''' = \frac{6(1-\alpha)}{d} \tag{46}$$

The vapor phase is heated by the wall and passes part of this heat to evaporate the liquid droplets. The vapor heating term in Eq. (29) is given as

$$q_v''' = \frac{4}{D} (q_{wv}'' + q_{r,wv}'' - q_{r,vd}'') - A_i''' q_{vd}'' \tag{47}$$

The interfacial drag on the droplets per unit volume is calculated by

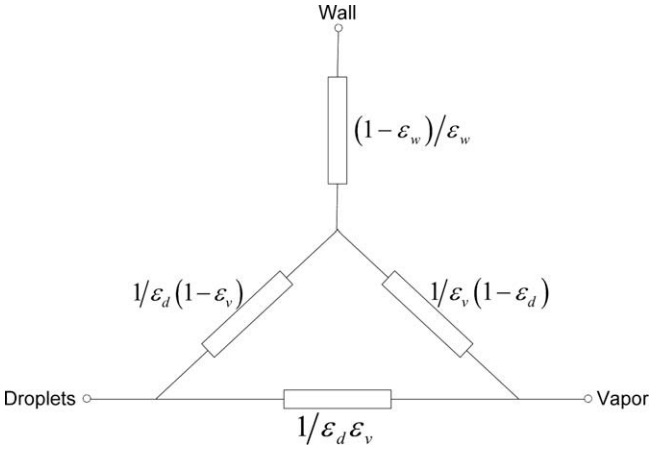

Fig. 3. Electrical analog of radiation heat transfer in dispersed flow region.

$$\tau_d''' = \frac{6(1-\alpha)F_D}{\pi d^3} \tag{48}$$

where F_D is the drag force on one droplets, which was suggested by Rowe (1961) as

$$F_D = \frac{C_D}{2}\rho_v |u_v - u_d|(u_v - u_d)\frac{\pi}{4}d^2 \tag{49}$$

here the drag coefficient is given as

$$C_D = \frac{24}{\mathrm{Re}_d}(1 + 0.15\mathrm{Re}_d^{0.687}) \tag{50}$$

In the current work, the droplet diameter is evaluated by the model of Kataoka et al. (1983):

$$d = 7.96 \times 10^{-3}\frac{\sigma}{\rho_v(\alpha u_v)^2}\mathrm{Re}_v^{2/3}\left(\frac{\rho_v}{\rho_l}\right)^{1/3}\left(\frac{\mu_v}{\mu_l}\right)^{2/3} \tag{51}$$

2.2.3. Pure vapor region

If the flow path is long enough, all the liquid droplets in the dispersed flow front will be evaporated eventually and the flow becomes pure vapor. In this study, when the void fraction reaches 0.99, the effect of the liquid phase is neglected and the flow is modeled as pure vapor, in which the only heat transfer mechanism is due to the forced convection to the vapor

$$q''_{wv} = 0.023\frac{k_v}{D}\mathrm{Re}_v^{0.8}\mathrm{Pr}_v^{0.33}(T_w - T_v) \tag{52}$$

2.2.4. Single-phase liquid region

When the tube wall has been chilled down to the rewetting temperature, intermittent liquid-wall contact is established and transition boiling begins. The transition boiling, characterized by rapid bubble generation, is highly unstable and immediately replaced by the nucleate boiling. Modeling the transition boiling region in chilldown is generally a difficult task, because the understanding and experimental data of the transition boiling are still very limited at the current stage. On the other hand, the transition boiling period in a chilldown process is so short and the heat flux of transition boiling is at the same order as that of the nucleate boiling, therefore nucleate boiling correlations are used to model both the transition boiling region and the nuclear boiling region in this work, as also adopted by other researches (Kawaji et al., 1988; Hedayatpour et al., 1993).

In the present study, Chen's correlation (Chen, 1966) for nucleate boiling is used, in which the total heat transfer coefficient equals to the sum of a microscopic (nucleate boiling) contribution h_{mic} and a macroscopic (bulk convection) contribution h_{mac}, in addition, h_{mic} is evaluated by pool boiling correlation times a suppression factor $S(\mathrm{Re}_{2\varphi})$; while h_{mac} is proposed to be enhanced from single-phase liquid convection with a enhancement factor $F(X_{tt})$. The Chen's correlation gives

$$h = h_{\mathrm{pool}}St(\mathrm{Re}_{2\phi}) + h_l F(X_{tt}) \tag{53}$$

where

$$h_{\mathrm{pool}} = 0.00122\left[\frac{k_l^{0.79}c_{pl}^{0.45}\rho_l^{0.49}}{\sigma^{0.5}\mu_l^{0.29}h_{lv}^{0.24}\rho_v^{0.24}}\right] \times (T_w - T_s(P_l))^{0.24}(P_s(T_w) - P_l)^{0.75} \tag{54}$$

$$h_l = 0.023\frac{k_l}{D}\mathrm{Re}_l^{0.8}\mathrm{Pr}_l^{0.4} \tag{55}$$

In Eq. (52), $\mathrm{Re}_{2\varphi}$ is the two-phase Reynolds number, X_{tt} is the Martinelli parameter.

In this study, the rewetting temperature is used as the transition criterion from the film boiling to nucleate boiling. Whenever the wall temperature is quenched below the rewetting temperature, the nucleate boiling will take over. The rewetting temperature is not a fixed value but affected by the flow rate, fluid and wall properties, etc. However, for the same experimental setup and limited range of working conditions, the rewetting temperature is generally a constant. Therefore, the rewetting temperature acquired from the experiments as the transition criterion is applicable to similar experimental conditions.

2.2.5. Tube wall temperature prediction

The wall temperature distribution is obtained by solving the 1D transient heat conduction equation:

$$\rho_w c_{p,w}\frac{\partial T_w}{\partial t} = k_w\frac{\partial^2 T_w}{\partial z^2} \tag{56}$$

in which T_w is the tube wall temperature, ρ_w, $c_{p,w}, k_w$ are the density, specific heat, and thermal conductivity of the tube wall, respectively.

The constitutive equations and heat transfer correlations used in the models above are basically independent of gravity as there is no gravity term involved. Furthermore, the equations and correlations are developed for axisymmetric cylindrical case that corresponds to the current case of inverted annular flow film boiling and dispersed flow boiling.

2.3. Numerical solution

A semi-implicit, finite difference scheme is used to discretize and solve the chilldown model. Very small time steps were used to avoid the instability that is inherent in the two-fluid model. The 1D heat conduction equation is solved with a total of 200 nodes. The solution procedure is illustrated in Fig. 4. First, the initial conditions for both the tube wall and the flow field are given, and the CHF location Z_{CHF} is set at the tube inlet. Then the calculation begins with an initial guess of α, P, u_l, u_v, h_v.

In this model, Post-CHF models are used for the downstream of the CHF point, while nucleate boiling model is applied to the upstream of CHF point. After solving the flow field, the wall temperature is updated according to Eq. (55). A pre-defined rewetting temperature is used as the transition criterion between the Post-CHF and nucleate boiling region. The location where the wall temperature becomes lower than the rewetting temperature is set as the new CHF location, and the program performed iterates until the wall temperature converges.

It is noted that in general, the rewetting temperature is not a fixed value but affected by the flow rate, fluid and wall properties, etc. However, for the same experimental setup and limited range of working conditions, the rewetting temperature is generally a constant. Therefore, using a constant rewetting temperature acquired from the experiments as the transition criterion is expected to be applicable to similar experimental conditions. Of course, a reliable correlation for rewetting temperature is desirable and will generalize the current chilldown model.

Additionally, in chilldown modeling we need one input from either quenching velocity or rewetting temperature. For example, in some other chilldown models (Kawaji and Banerjee, 1988; Hedayatpour et al., 1993) the rewetting temperature is not fixed, but the location and the propagation of the quenching front are considered *a priori*. These models begin with the IAFB and move back to the upstream of the quenching front after solving the Post-CHF region. In our model, setting the rewetting temperature as a known quantity requires less information from the experiments and therefore simplifies the model.

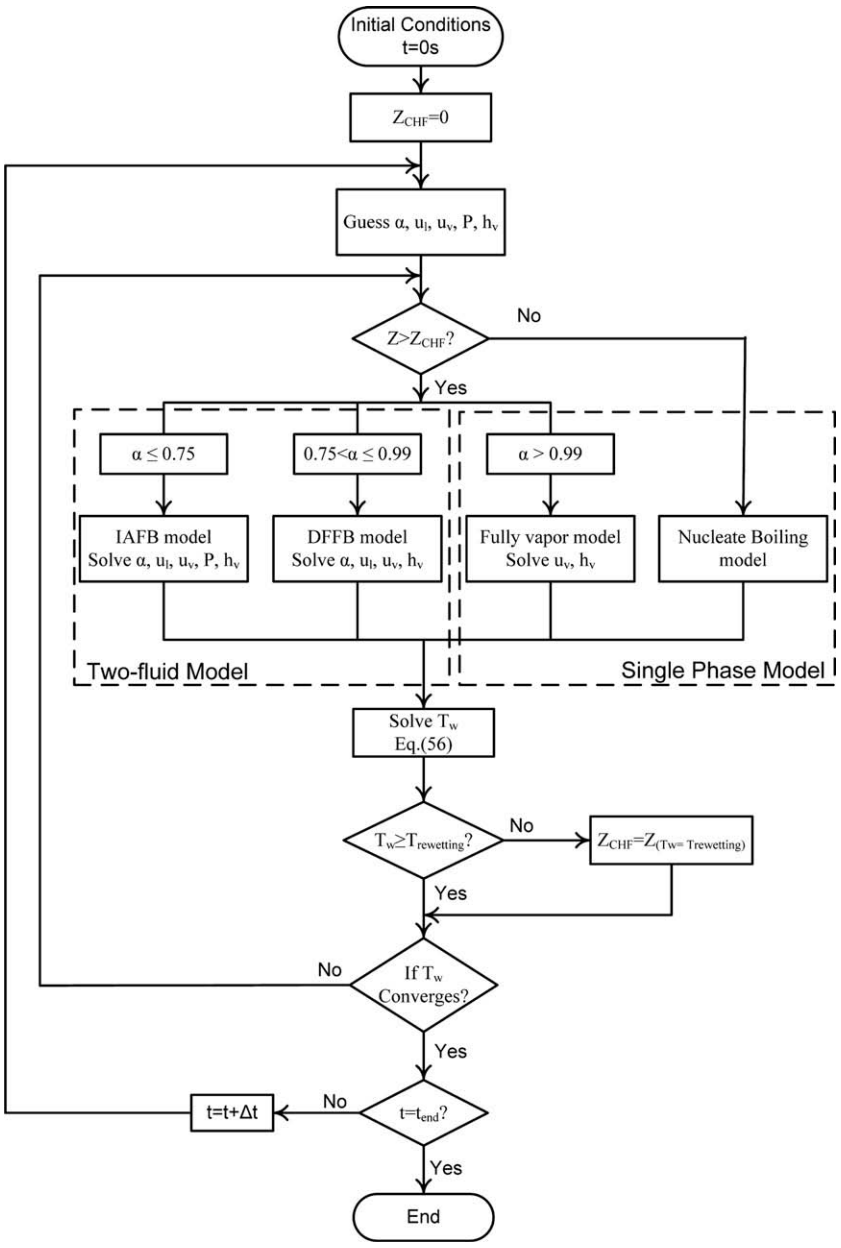

Fig. 4. Solution procedure of the cryogenic chilldown model.

3. Model validation, numerical results and discussion

Before the code was used for the chilldown problem, it was validated in two ways. First, the grid independence of the code was tested. Next, the code was used to simulate a dam-break problem and the computational results were compared with the analytical solution (Zoppou, 2003). Validation results show that this code is reliable and accurate. Then the model was used to simulate a real cryogenic chilldown process and the results were compared with previous experimental results.

In the literature, to the authors' best knowledge, the only experimental investigation that covered the whole cryogenic chilldown process under a reduced gravity environment was conducted by Antar and Collins (1997). Their work is summarized as follows. The low gravity environment, which had an average gravitational acceleration of ±0.01 g, was provided by a NASA KC-135 aircraft. Two different test sections were used in the experiments. A quartz tube, having 1.275 cm OD and 1.05 cm ID and roughly 60 cm length, was used for the purpose of recording the images of flow regimes; while the stainless steel test section was used for wall temperature measurement. The stainless steel test section, which has the dimension of 0.635 cm OD, 0.432 cm ID, and 70 cm length, is modeled in the current study. Both test sections were mounted vertically inside a vacuum jacket. Saturated liquid nitrogen was injected from the bottom of the test section, while the top of the test section was opened to the atmosphere.

The two main variables in the experiment were the nitrogen flow rate and the initial tube temperature. The tube was initially at the room temperature, after each test the wall temperature was always brought to above 0 °C. Two type-T thermocouples were soldered to the outside wall of the stainless steel test section located at 20 cm and 30 cm from the inlet, respectively. The temperature measurements show that the rewetting temperature is relatively a constant, which is about 115 K, for the experimental flow rate range. The wall temperature drops very quickly at this point. Therefore, the transition criterion from film to nucleate boil-

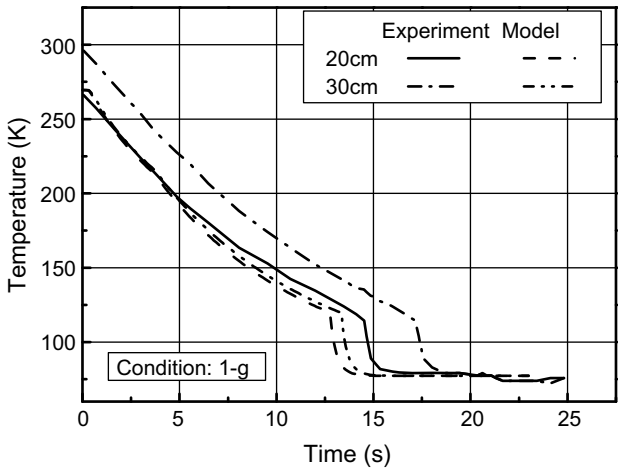

Fig. 5. Comparison between measured and predicted wall temperatures under 1-g condition with flow rate of 40 cc/s.

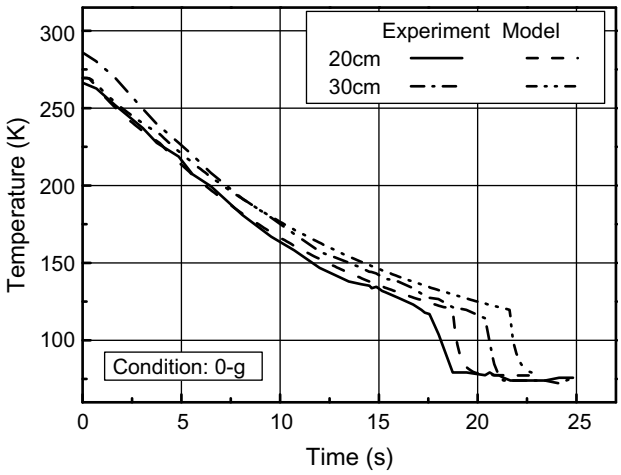

Fig. 6. Comparison between measured and predicted wall temperatures under 0-g condition with flow rate of 40 cc/s.

ing is set as 115 K. The transition boiling period is found to be very short and usually less than one second.

Fig. 5 shows the measured and predicted wall temperatures under the 1-g condition with a flow rate of 40 cc/s. The model slightly over-predicts the rate of temperature decrease before the rewetting point and thus leads to an earlier transition to the nucleate boiling region, the overall agreement is good. It should be pointed out that for the experimental curves in Fig. 5 there was an initial tube wall temperature difference of 30 °C between the 20 cm (266 °C) and 30 cm (296 °C) locations. In our model, however, the tube wall was assumed to have a uniform wall temperature initially; therefore both 20 cm and 30 cm locations have the same initial temperature. It is noted that all four curves have similar slopes (rate of cooling), as a result, the experimental quenching times for 20 cm and 30 cm locations are different while the model results are close.

Comparison between experimental data and model prediction in microgravity condition is illustrated in Fig. 6. Again, a good agreement is achieved. In Fig. 6 for microgravity, the initial temperature difference between the two locations (about 17 °C) is smaller than that for 1g (30 °C) in the experimental case. The heat transfer rate is generally lower under microgravity condition, therefore as compared with the 1-g case, the quenching time is longer in microgravity. The four curves again have very similar slopes in Fig. 6. These are the reasons that the model predictions and the experimental data are closer under microgravity. More specifically, the model underestimates the rate of temperature decrease very slightly. This discrepancy is believed to have come from the residual gravity effect in the experiment. The experiment was performed in a KC-135 aircraft and the authors reported that the residual gravity is in the range of ±0.01 g (Antar and Collins, 1997). Based on the gravity effects discussed in relevance to Fig. 8b below, the estimated discrepancy should be about 5% in the wall temperature history curves in Fig. 6 for 0.01 g versus zero gravity. The actual discrepancy between the measured data and our model results in Fig. 6 is about 12%. The larger discrepancy in the actual case is probably due to the plus and minus 0.01 g fluctuation in the KC-135 experiment. It is important to note that the slopes of the quenching curves predicted by our model are the same as those from the experiments for both 1-g and 0-g, which virtually verifies the model.

A given tube wall location could potentially experience a pure vapor flow, dispersed flow, inverted annular flow or nucleate boil-

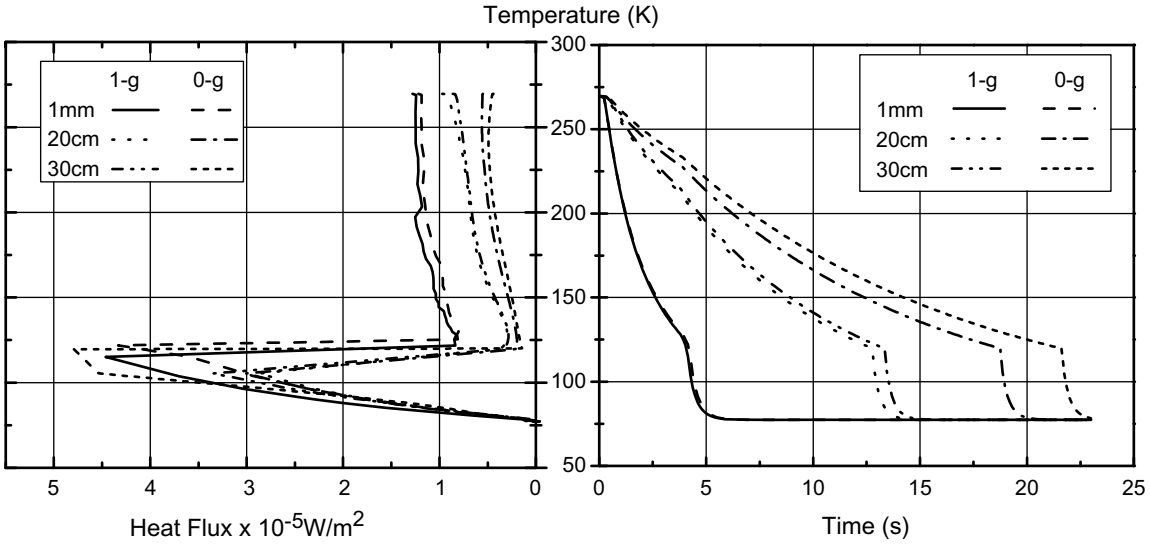

Fig. 7. Model prediction of boiling curve (a) and wall temperatures (b) at different axial locations under both 1-g and 0-g conditions.

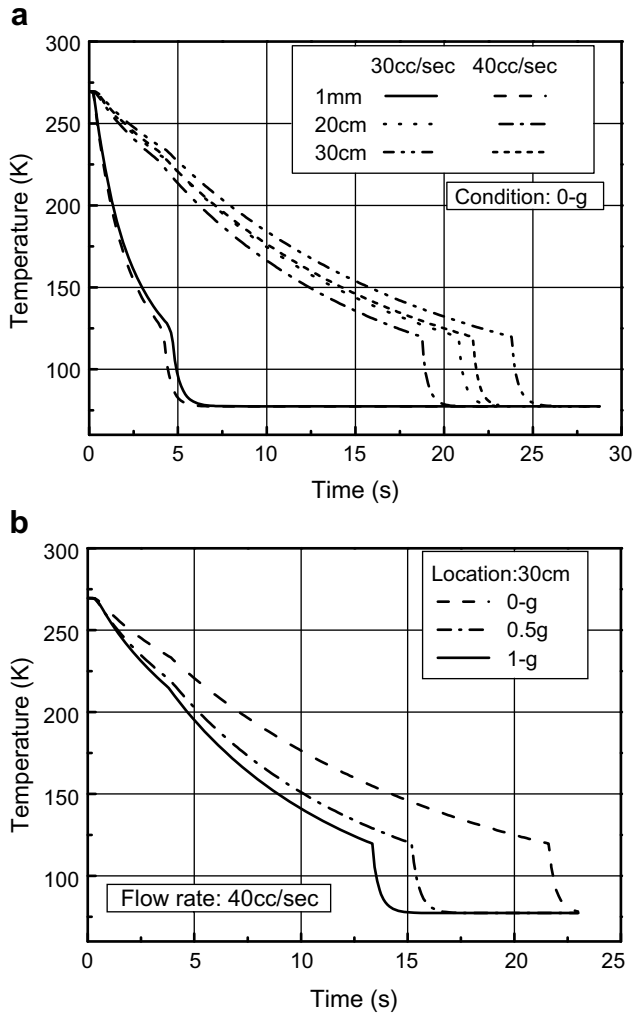

Fig. 8. Effects of inlet flow rate and gravity level on chilldown process: (a) effect of inlet flow rate (b) effect of gravity level.

ing. Under the microgravity condition, the durations for both dispersed flow and inverted annular flow are longer than those under the normal gravity condition. This is because heat transfer rate is reduced under microgravity. Also, since the two-phase flow is heated along the tube, the location which is closer to the inlet will experience a shorter film boiling time. For the thermocouple located at the 30 cm location in Fig. 6, complete vapor flow only lasts about 0.2 s; dispersed flow regime ends at about 0.5 s; inverted annular flow is much longer and ends at about 21 s.

Right part of Fig. 7 shows the prediction of the transient wall temperatures at different axial locations along the tube under both 1-g and 0-g conditions with a flow rate of 40 cc/s. The corresponding boiling curves are shown on the left part of Fig. 7. The three selected locations are 1 mm, 20 cm and 30 cm from the inlet, respectively. Obviously, the tube wall closer to the inlet is quenched much more quickly. Moreover, the gravity effect is found to be less important near the tube inlet (1 mm line), because the void fraction is very small there and the flow is almost a single-phase liquid. The gravity effect is found to increase along the axial direction.

Effects of the inlet flow rate and gravity level are illustrated in Fig. 8. As seen from Fig. 8a, a higher flow rate is associated with a quicker temperature decrease, and this effect is more important further downstream. Fig. 8b illustrates that in the film boiling region the heat transfer rate decreases with decreasing gravitational acceleration for the bottom flooding case.

Merte (1990) reported terrestrial and microgravity pool boiling data for saturated liquid nitrogen under atmospheric pressure. For pool film boiling, based on Fig. 26 in Merte (1990), the estimated average heat transfer coefficients are 50 W/m^2 K and 125 W/m^2 K for microgravity and terrestrial gravity, respectively. From Fig. 8b, for inverted annular flow film boiling, the corresponding heat transfer coefficients are calculated as follows:

Wall temperature $T = 250$ K $\quad h(1\text{ g}) = 450$ W/m^2 K

$h(0\text{ g}) = 272$ W/m^2 K

Wall temperature $T = 177$ K $\quad h(1\text{ g}) = 592$ W/m^2 K

$h(0\text{ g}) = 350$ W/m^2 K

According to the comparison, irrelevant of either pool or flow boiling, heat transfer coefficient is smaller under microgravity than that in earth gravity by 40% and 60% for flow and pool boiling, respectively.

Fig. 9 gives the wall temperature profiles at different times. Wall temperature decreases with time and increases along the axial direction. At the beginning, the maximum temperature gradient is at the tube inlet, when QF appears, the maximum temperature gradient moves with the QF.

Based Fig. 9, the quench front propagated little in the first 15 seconds while the tube wall temperatures above the quench front were falling uniformly at about the same rate. So, when the tube wall temperature in the unquenched region approaches 115 K, the quench front would be predicted to suddenly propagate and the entire tube to be subsequently quenched in a very short time that is consistent with the results obtained by Westbye et al. (1995) in microgravity.

The predicted void fractions at different times under 0-g condition are displayed in Fig. 10. The void fraction increases along the axial direction since more and more liquid is evaporated as the flow propagates. In the initial stage, the wall is very hot, the void fraction shows an abrupt increases along the axial direction, and the flow regime changes from IAF to dispersed flow and then to pure vapor flow. Later on, the pure vapor region and dispersed region are totally pushed out of the tube and the exit state of the two-phase flow is in IAFB, and finally QF appears and sweeps towards downstream.

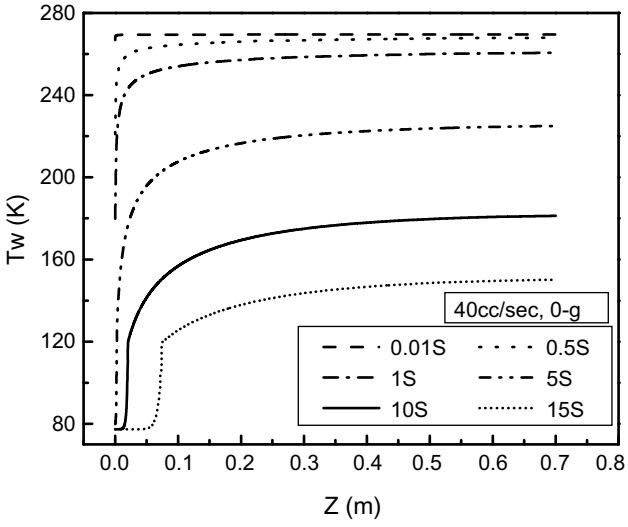

Fig. 9. Wall temperature profiles at different time.

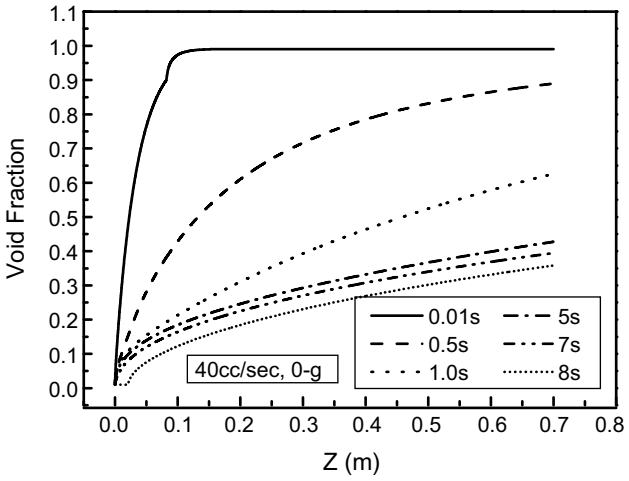

Fig. 10. Void fraction along the tube during chilldown.

After 8 seconds, the void fraction above the quench front was predicted to fall to less than 30% everywhere. Under such a low void fraction, the dispersed droplet flow is ruled out, and an inverted annular flow would be predicted to exist over the entire tube with a continuous liquid core occupying more than 80% of the tube diameter.

4. Conclusions

In the present study, a two-fluid model is developed to describe the transient cryogenic chilldown process under both terrestrial and microgravity conditions. According to the experimental observation, four distinct flow regions are incorporated in the model, which are single-phase vapor flow, dispersed flow, inverted annular flow, and single-phase liquid flow. For each flow region, different heat mechanism is established. The model results show a good agreement with both 1-g and microgravity experimental data. It is found that the gravity effect increases along the axial direction as the two-phase flow quality increases. In the film boiling region the heat transfer rate decreases with decreasing gravitational acceleration for the bottom flooding case.

Acknowledgments

This research was supported by the NASA Hydrogen Research for Spaceport and Space Based Applications at the University of Florida (Grant No. NAG3-2930). The support by the Andrew H. Hines, Jr./Progress Energy Endowment Fund is also acknowledged. We appreciate the meaningful discussion with Professor Renwei Mei and Dr. Jun Liao.

References

Analytis, G.T., Yadigaroglu, G., 1987. Analytical modeling of inverted annular film boiling. Nuclear Engineering and Design 99, 201–212.
Andreani, M., Yadigaroglu, G., 1994. Prediction methods for dispersed flow film boiling. International Journal of Multiphase Flow 20 (Suppl), 1–51.
Antar, B.N., Collins, F.G., 1997. Flow boiling during quenching in low gravity environment. International Journal of Microgravity Science and Technology 3, 118–128.
Bolle, L., Moureau, J.C., 1986. Spray cooling of hot surface. Multiphase Science and Technology. vol. 1. Hemisphere, Publishing, Washington, DC. pp. 447–456.
Bronson, J.C., Edeskuty, F.J., Fretwell, J.H., Hammel, E.F., Keller, W.E., Meier, K.L., Schuch, A.F, Willis, W.L., 1962. Problems in cool-down of cryogenic systems. Advances in Cryogenic Engineering 7, 198–205.
Burke, J.C., Byrnes, W.R., Post, A.H., Ruccia, F.E., 1960. Pressure cooldown of cryogenic transfer lines. Advances in Cryogenic Engineering 4, 378–394.
Chen, J.C., 1966. Correlation for boiling heat transfer to saturated fluids in convective flow. Industry Engineering Chemistry Process Design and Development 5, 322–329.
Chen, J.C., Ozkaynak, F.T., Sundaram, R.K., 1979. Vapor heat transfer in post-CHF region including the effect of thermodynamic non-equilibrium. Nuclear Engineering and Design 51, 143–155.
Chi, J.W.H., 1965. Cooldown temperatures and cooldown time during mist flow. Advances in Cryogenic Engineering 10, 330–340.
Chan, A.M.C., Banerjee, S., 1981a. Refilling and rewetting of a hot horizontal tube Part II: structure of a two-fluid model. ASME Journal of Heat Transfer 103, 287–292.
Chan, A.M.C., Banerjee, S., 1981b. Refilling and rewetting of a hot horizontal tube Part III: application of a two-fluid model to analyze rewetting. ASME Journal of Heat Transfer 103, 653–659.
Ganić, E.N., Rohsenow, W.M., 1977. Dispersed flow heat transfer. Intentional Journal of Heat and Mass Transfer 20, 855–866.
Guo, Y.J., Mishima, K., 2002. A non-equilibrium mechanistic heat transfer model for post-dryout dispersed flow regime. Experimental Thermal and Fluid Science 26, 861–869.
Hammouda, N., Groeneveld, D.C., Cheng, S.C., 1997. Two-fluid modeling of inverted annular film boiling. International Journal of Heat and Mass Transfer 40, 2655–2670.
Hedayatpour, A., Antar, B.N., Kawaji, M., 1993. Cool-down of a vertical line with liquid nitrogen. AIAA Journal of Thermophysics and Heat Transfer 7, 426–434.
Incropera, F.P., DeWitt, D.P., 2002. Fundamentals of Heat and Mass Transfer, fifth ed. John Wiley & Sons, New York.
Kataoka, I., Ishii, M., Mishima, K., 1983. Generation and size distribution of droplet in annular two-phase flow. ASME Journal of Fluid Engineering 105, 230–238.
Kataoka, I., Ishii, M., 1983. Entrainment and deposition rates of droplets in annular two-phase flow. In: Proceedings of ASME/JSME Thermal Engineering Joint Conference, vol. 1.
Kawaji, M., Ng, Y.S., Banerjee, S., Yadigaroglu, G., 1985. Reflooding with steady and oscillatory injection: Part I-flow regimes, void fraction, and heat transfer. ASME Journal of Heat Transfer 107, 670–678.
Kawaji, M., Banerjee, S., 1987. Application of a multifield model to reflooding of a hot vertical tube Part I: model structure and interfacial phenomena. ASME Journal of Heat Transfer 109, 204–211.
Kawaji, M., Banerjee, S., 1988. Application of a multifield model to reflooding of a hot vertical tube Part II: analysis of experimental results. ASME Journal of Heat Transfer 110, 710–720.
Kawaji, M., Westbye, C.J., Antar, B.N., 1991. Microgravity experiments on two-phase flow and heat transfer during quenching of a tube and filling of a vessel. AIChE Symposium Series 87 (283), 236–243.
Kays, W.M., 1993. Convective Heat and Mass Transfer. McGraw-Hill, New York.
Laverty, W.F., Rohsenow, W.M., 1967. Film boiling of saturated nitrogen flowing in a vertical tube. ASME Journal of Heat Transfer 91, 90–98.
Lee, K., Ryley, D.J., 1968. The evaporation of water droplets in superheated steam. ASME Journal of Heat Transfer 90, 445–451.
Liao, J., 2005. Modeling two-phase transport during cryogenic chilldown in a pipeline. Ph.D. Dissertation, University of Florida.
Merte, H. 1990. Nucleate pool boiling in variable gravity, in low-gravity fluid dynamics and transport phenomena. In: Koster, J.N., Sani, R.L. (Eds.), Progress in Astronautics and Aeronautics. vol. 130, pp. 15–72.
Rowe, P.N., 1961. Drag forces in a hydraulic model of a fluidised bed, Part II. Transactions of the Institute of Chemicals Engineers 39, 175–180.
Sun, K.H., Gonzalez-Santalo, J.M., Tien, C.L., 1976. Calculations of combined radiation and convection heat transfer in rod bundles under emergency cooling conditions. ASME Journal of Heat Transfer 98, 414–420.
Tian, W.X., Qiu, S.Z., Jia, D.N., 2006. Investigations on post-dryout heat transfer in bilaterally heated annular channels. Annals of Nuclear Energy 33, 189–197.
Westbye, C.J., Kawaji, M., Antar, B.N., 1995. Boiling heat transfer in the quenching of a hot tube under microgravity. AIAA Journal of Thermophysics and Heat Transfer 9, 302–307.
Yuan, K., Ji, Y., Chung, J. N., 2005. Cryogenic two-phase flow and heat transfer under terrestrial and micro gravity. In: Proceedings of 2005 ASME International Mechanical Engineering Congress (IMECE).
Yuan, K., Ji, Y., Chung, J.N., 2007. Cryogenic chilldown process under low flow rates. International Journal of Heat and Mass Transfer 50, 4011–4022.
Zoppou, C., Roberts, S., 2003. Explicit schemes for dam-break simulations. Journal of Hydraulic Engineering 129, 11–34.